IJES *Iranian Journal of Earth Sciences*
Vol. 11, No. 2, 2019, 126-140.

Eocene-Oligocene volcanic units of momen abad, east of Iran: petrogenesis and magmatic evolution

Sahar Tarabi[1], Mohamad-Hashem Emami*[2], Soroush Modabberi[3], Seyed-Jamal Sheikh-Zakariaee[1]

1. Department of Geology, Science and Research Branch, Islamic Azad University, Tehran, Iran
2. Department of Geology, Islamshahr Branch, Islamic Azad University, Tehran, Iran
3. School of Geology, College of Science, University of Tehran, Tehran, Iran

Received 20 May 2018; accepted 17 November 2018

Abstract

This study investigates petrology and major, minor, and rare earth elements geochemistry of East Iranian Eocene–Oligocene volcanic rocks in Sistan suture zone, to examine their petrogenesis and magma evolution. The volcanic rocks include andesite, trachy-andesite, dacite and rhyolite. These calc-alkaline rocks of high-K series are enriched in Large Ion Lithophile Elements of Rb and Ba and depleted in High Field Strength Elements (e.g. Ti and Nb). The REE pattern shows Eu negative anomaly. These features are comparable with rocks in subduction zone of continental margin setting. The petrographic features and the geochemical variation of major oxides and trace elements against SiO_2 can be related to fractional crystallization in parent magma. The trace element ratios, e.g. Nb/La, Nb/U, Ba/Rb, Nb/Y and Rb/Y, verify crustal contamination with a remarkable upper crustal contamination as the main process in the formation of volcanic series. The ratios of Nb/Ba and Nb/Zr indicate that magmatic activity in Momen Abad had resulted from sub-continental lithospheric mantle. In addition, Nb/Y and Zr/Yb versus Ta/Yb reveals an E-MORB like mantle source. A spinel lherzolite composition with significant role of the AFC processes are deduced from the concentrations of Yb and Y, and the ratios of Th/Yb and La/Yb. The Ba/Nb, Ba/Th and Th/Nb ratios presume a metasomatized mantle source resulted from the melting of upper crust sediments inherited from the subduction of Neotethys ocean beneath the Lut Block.

Keywords: *Volcanics, Rare Earth Elements (REE), Fractional crystallization, East of Iran, Momen Abad.*

1. Introduction

The Cenozoic magmatism in Eastern Iran and especially in the Sistan suture zone is one of the most extensive magmatic activities in Iran which is manifested by the Eocene-Oligocene calc-alkaline volcanism and the Quaternary alkaline basaltic volcanism (Pang et al. 2012). Sistan suture zone with a roughly N-S trend has been formed due to the closure of a small oceanic branch of the Neo-Tethys Ocean which had been formed as a result of divergence of Lut Block toward west and the Afghan block toward east in the Late Cretaceous (Camp and Griffis 1982; Tirrul et al. 1983). The geodynamic model of the study area is completely ambiguous. However, various theories have been proposed by scholars. Formation of the island arc during the Late Cretaceous has been attributed to the eastward subduction of an oceanic plate beneath the Afghan Block (Camp and Griffis 1982; Tirrul et al. 1983), westward subduction beneath the Lut Block (Berberian 1983; Zarrinkoub et al. 2012), two-sided subduction (Arjmandzadeh et al. 2011), eastward intra-oceanic subduction (Saccani et al. 2010) and northward to eastward subduction (Verdel et al. 2011) . Nevertheless, the subduction and the formation of volcanic arcs and subsequently the closure of the Neo-Tethys ocean took place in Late Cretaceous resulted in the Eocene-Oligocene calc-alkaline volcanism.Pang et al. (2012) attributed the volcanism to delamination of a thickened lithospheric root and suggested that magmatism is inherited from the Earth's mantle with minor contribution of sediments through partial melting also the fluids liberated from the subducting plate (Pang et al. 2013). This research evaluates the magmatic evolution in Momen Abad volcanic zone including the effect of Assimilation-Fractional Crystallization (AFC) processes of the modified mantle source on the petrogenesis of andesite, dacite and rhyolite.

*Corresponding author.
E-mail address (es): hashememami@yahoo.com

2. Geology of the study area

Momen Abad area is located in East Iran, in southeast of Birjand and 15 km northeast of Sarbisheh (N 32°34′28″ - 32°43′25″ and E 59°49′52″ - 60°00′00″) in the South Khorasan province, Iran (Figs 1 and 2). According to Stocklin (1968) and other scholars (Camp and Griffis 1982; Tirrul et al. 1983) the study area is a part of Sistan suture zone. According to the geological map of the area (Nazari and Salamati 1999), the siltstone-shale and sandstone outcrops along with interbedded conglomerate, silty limestone and marls (PeE^m, PeE^{ph} and PeE^s units in Fig 2) with the age of Paleocene and Eocene are supposed to be formed in a fore-arc basin setting (Nazari and Salamati 1999).

The magmatic suite consists of calc-alkaline volcanic rocks with the age of Eocene, Oligocene, Miocene and

Pliocene and widely dispersed Quaternary alluvial deposits (Fig 2). The main volcanic rocks in the study area are calc-alkaline in nature including: acidic and intermediate calc-alkaline lavas of andesite-trachy-andesite, andesite to pyroxene andesite, perlitic rhyolite, pyroclastic unit, tuff, brecciated ignimbrite and dacite-rhyodacitic tuff with the age of Eocene-Oligocene and Miocene.

Altered and brecciated volcanic series (Eo^{br}) with intermediate to acidic composition are in juxtaposition with andesite, pyroxene andesite and dacitic tuff by a faulted contact. The pyroclastic units of T^{tm} with andesite composition and a perlitic matrix and volcanic breccia texture are located beneath the An_2 unit. The andesite and trachy andesite units (An_2) appear in an uneven morphology in the region. The andesite and pyroxene-andesite units (Eo^{ba} and Eo^{ap}) are found in contact with the altered and brecciated volcanic units (Eo^{br}) with myriad of fracture systems in the region.

The perlitic-rhyolite units (Om^{Pr}) are comprised of brown to black glass which are notably appear in the altered tuffs in the area. The dacite and dacitic tuff unit (Om^{da2}), expressed in white to gray, shows the highest percentage of argillic alteration. Dark brown and black units of andesite-basalt to pyroxene andesite (unit b) are found in less abundance along with the volcanic glass.

Basaltic andesite overlays white tuffs and other units such as T^{tm}, Pl^{c}, and Eo^{br} with an unconformity surface. Pl^{c} unit is comprised of conglomerate and sandstone which outcropped in the northwest part of the study area. PlQ^{c} unit consists of a polygenetic conglomerate overlaying the Pl^{c} conglomerate unit. They are Eocene, Oligocene and Miocene in age and are widely spread across the eastern part of the study area, while the western part includes old alluvium, alluvial fan and Quaternary deposits such as sandstone and gravels.

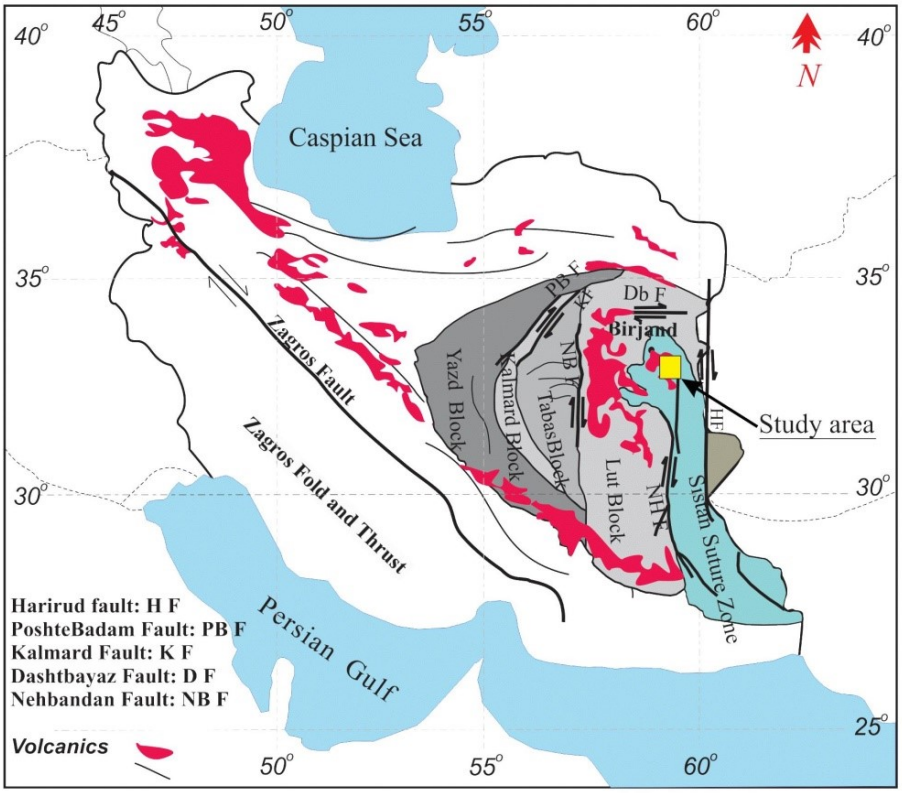

Fig 1. Structural subdivision of Iran and location of the Momen Abad area in East Iran (Modified after Aghanabati 2004).

3. Sampling and analytical methods

One hundred samples were collected from the study area during three field excursions in 2016-2017 to cover the Om^{pr}, Om^{dr2}, Eo^{ba}, Eo^{ap}, Eo^{br}, and An_2 unit in the study area, 40 samples from andesites, 35 dacites, and 25 hyolites based on the field observation. The samples were among the fresh outcrops and the weathered rims of the samples were removed before packing in plastic sample bags.

Eighty thin-sections were prepared in Tarbiat Modares University of Tehran, and were studied by using Zeiss polarizing microscope in the Islamic Azad University, Science and Research Branch, Tehran. A number of 20 rock samples with least alteration were selected for geochemical analyses. The samples were powdered to 75µm after air drying in the oven to a temperature of 110ºC. The powders were placed in plastic bags and

were transferred to the SGS Laboratory, South Africa for geochemical analysis.
The concentrations of 43 elements were determined by Inductively Coupled Plasma-Atomic Emission Spectrometry (ICP-AES) (for major elements) and ICP-MS (for trace elements) following lithium-borate fusion of a 1 to 3g of the sample. Loss on ignition (LOI) was determined as the weight difference after ignition at 1000°C. Data were interpreted using Igpet, GCDkit and Corel Draw softwares.

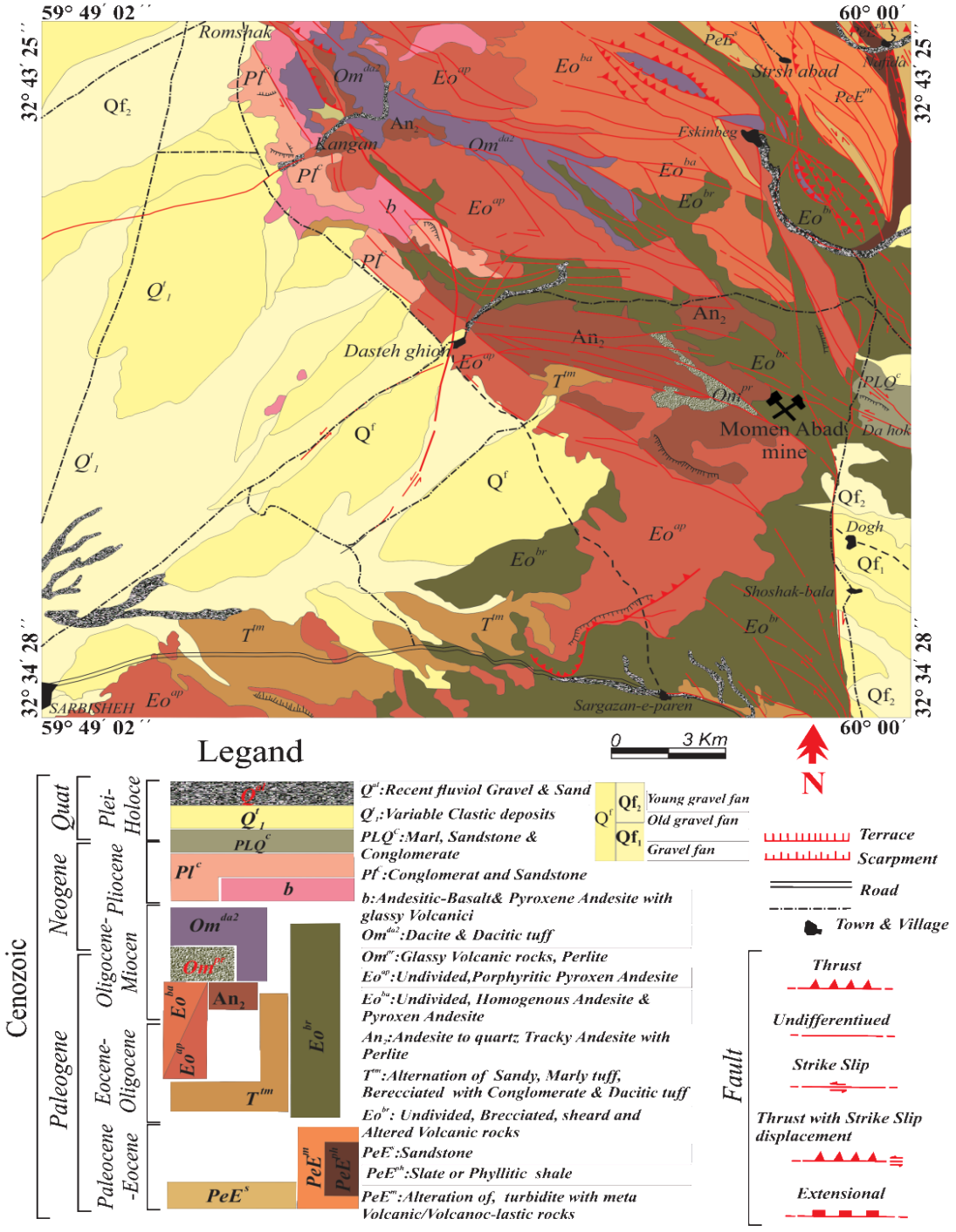

Fig 2. Geological map of the Momen Abad area (Redrawn after Nazari and Salamati 1999).

4. Petrography

Based on the petrographic studies, the volcanic rock units of the Momen Abad area are comprised of acidic to intermediate calc-alkaline lavas typically andesite, dacite and rhyolite displaying the following petrographic features:

Andesite: Plagioclase phenocrysts are the main mineral constituents and clinopyroxene and amphibole are the most common mafic minerals in these rocks. About 70 to 75% of the total volume of the rocks is comprised of plagioclases (25µm to 1 cm in size) (Fig 3a). Based on the extinction angle and refractive indices, this mineral is recognized as labradorite to andesine members of the plagioclase series. Pyroxenes with a broad size ranging from 25 to 780µm account for 20 to 25 % of the total mineral composition (Fig 3b). Amphibole group minerals occurring as brown hornblende show a size range of 25 to 980µm explain 5 to 15% of minerals (Fig 3c). The rock matrix is composed of plagioclase, pyroxene, opaque minerals and glass. These rocks can be classified as pyroxene andesite and amphibole pyroxene andesite in samples with significant percentage of pyroxene and amphibole minerals.

Andesite-trachy andesite: Plagioclase phenocrysts ranging in size from 25µm to 1cm are the main rock-forming minerals comprising about 70 to 80% of these rocks. Alkali feldspars are rarely found as phenocrysts and occur predominantly in the rock matrix. Pyroxene as the common mafic mineral and with the grain sizes ranging from 25 to 380µm, accounts for 25 to 30% of the rock minerals (Fig 3b). The rock matrix is composed of plagioclase, alkali feldspar, pyroxene, secondary opaque minerals, iron oxides and commonly brown volcanic glass.

Dacite: Plagioclase phenocrysts, quartz and alkali feldspars are the main rock-forming minerals and pyroxenes are the predominant mafic mineral in these rocks. Plagioclase minerals with a wide range of grain size (from 25 up to 980µm) constitute more than half of the rock minerals. Quartz as microlite and phenocryst (15 to 680µm in size) represents about 20 to 30% of the rock. Similarly, microlites and phenocrysts of alkali feldspars with the respective minimum and maximum sizes of 35µm and 880µm form 20 to 25% of the rocks. Small amounts of pyroxene minerals are also found as phenocrysts (25 to 760µm in size) as well as microphenocrysts.

Rhyolite: Quartz with ranging in size from 25 to 280µm is the main mineral constituent of these rocks. Subsequently, plagioclase and alkali feldspars account for 20-25% and 10% of the total minerals, respectively. Plagioclase grain size ranges from 15 to 980µm. Alkali feldspars are commonly sanidine, 25 to 680µm in size and with a distinct Carlsbad twinning (Fig 3e-f). Pyroxene and biotite comprise about 5 to 10% and amphibole forms 5% of the minerals. Perlitic texture is the most remarkable microstructure in rhyodacite-rhyolite rocks.

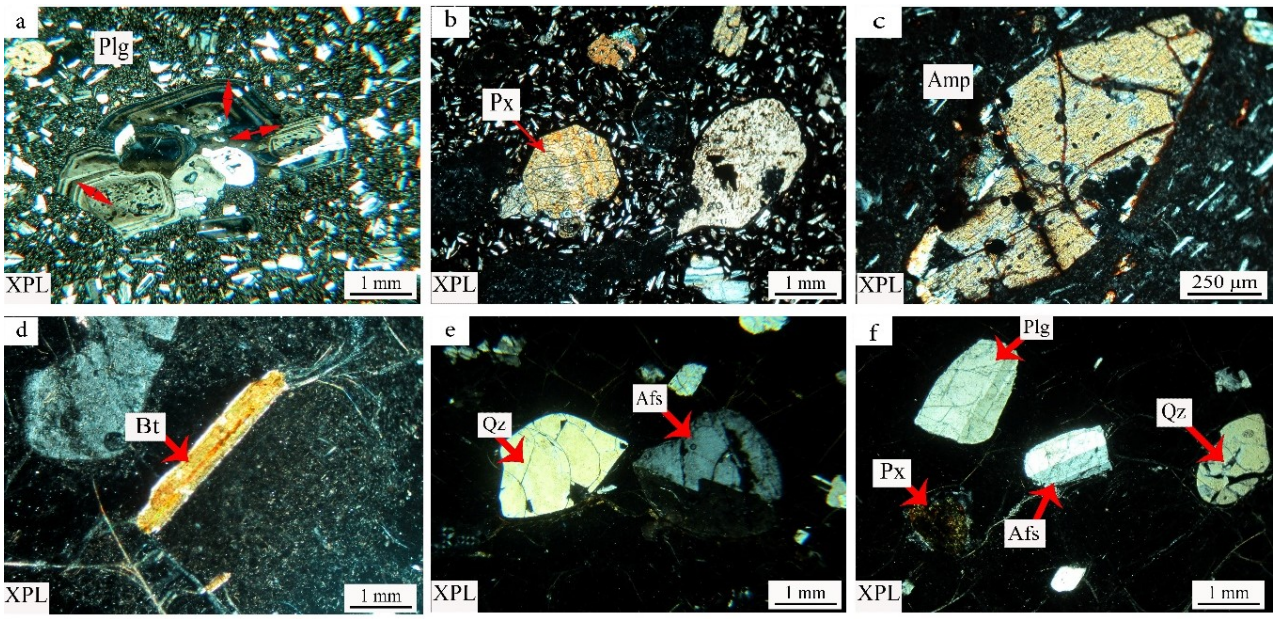

Fig 3. The main minerals and common mafic minerals in the rock sequence of the study area. a) Plg (plagioclase), b) Px (pyroxene), c) Amp (amphibole), d) Bt (biotite), e-f) Qz (quartz) and Afs (alkali feldspar).

5. Geochemical characteristics

The trace and rare earth element geochemistry combined with the petrographic analysis are important determining tools to elucidate the origin and magmatic evolution of igneous rocks (Litvak et al. 2015).

Table 1 presents the geochemical analysis results for major, trace and rare earth element composition of volcanic rock types in this region. All major oxides are volatile-free normalized to 100%.

The contents of major oxides in andesite and dacite samples are as follow (Table 1): SiO_2 (61.96-68.90), TiO_2 (0.60-0.91), Al_2O_3 (14.93-17.40), CaO (3.34-5.97). The concentration of SiO_2, TiO_2, Al_2O_3 and CaO in rhyolite samples varies in the range of 70.71- 79.46, 0.15- 0.54, 11.06-13.66 and 0.59-3.17, respectively.

In the total alkali versus silica (TAS) diagram (Le Bas et al. 1986), the samples fall in the fields of basaltic trachy-andesite, trachyte, andesite, dacite and rhyolite (Fig 4a). According to the AFM diagram (Irvine and Baragar 1971), the samples are grouped within the calc-alkaline series field (Fig 4b). With respect to the SiO_2 versus K_2O classification grid proposed by (Peccerillo and Taylor 1976), majority of the samples fall in the high-K series and some show calc-alkaline affinity (Fig 4c).

Table 1. Concentration of major oxides (in wt%) and trace elements (in ppm) in the analyzed rock samples.

Rock Type	Andesite				Dacite				Rhyolite	
Sample Name	T.F.An-18	T.F.An-22	T.S.V-112	T.S.V-117	T.F.P-30	T.S.V-100	T.S.V-106	T.S.V-108	T.S.V-63	T.S.V-97
SiO_2	61.96	63.12	62.98	63.04	67.44	68.90	67.40	64.94	76.41	71.41
Al_2O_3	17.40	16.95	16.83	16.50	17.30	14.93	15.95	16.23	12.72	13.40
CaO	5.97	5.19	4.93	5.03	3.34	3.34	3.49	4.47	0.96	2.58
MgO	2.96	2.52	2.64	2.95	0.94	1.04	1.58	2.70	0.32	0.25
Na_2O	3.61	3.67	4.00	3.89	4.32	2.55	3.53	3.63	3.52	3.34
K_2O	2.11	2.41	2.49	2.60	3.05	4.68	3.77	2.94	4.42	4.03
Cr_2O_3	0.01	0.01	0.01	0.02	0.01	0.01	0.01	0.02	0.01	0.01
TiO_2	0.89	0.89	0.91	0.87	0.61	0.82	0.60	0.72	0.17	0.54
MnO	0.09	0.07	0.09	0.09	0.05	0.05	0.07	0.07	0.02	0.09
P_2O_5	0.24	0.29	0.26	0.25	0.18	0.19	0.15	0.17	0.01	0.15
SrO	0.02	0.03	0.02	0.02	0.02	0.01	0.01	0.03	0.01	0.02
BaO	0.04	0.04	0.05	0.04	0.05	0.05	0.05	0.05	0.04	0.04
Fe_2O_3	2.41	2.45	2.46	2.41	2.15	2.37	2.14	2.26	1.71	2.08
LOI	1.81	4.89	1.99	1.72	3.41	2.78	2.33	2.69	2.01	2.73
Ba	319	332	403	343	446	452	417	397	321	374
Ce	51.2	48.6	57.8	54.2	67.3	61.1	66.2	60.4	67.5	53.5
Cr	80	60	70	90	20	20	60	90	30	30
Cs	5.21	2.45	6.23	5.33	8.66	5.93	14.00	9.05	14.25	4.39
Dy	3.76	3.67	4.15	4.22	3.93	4.06	4.06	3.83	4.78	3.98
Er	2.18	2.38	2.88	2.61	2.78	2.46	2.63	2.73	3.02	2.65
Eu	1.13	1.08	1.18	1.16	1.02	1.17	0.81	0.89	0.49	0.98
Ga	17.0	14.2	17.6	16.7	16.9	18.2	18.0	17.7	14.5	15.2
Gd	3.92	3.93	4.39	4.29	4.12	4.55	3.95	4.06	4.42	3.95
Hf	4.4	4.9	6.0	4.9	6.7	6.1	5.5	6.3	5.2	5.1
Ho	0.80	0.81	0.90	0.85	0.89	0.88	0.82	0.84	1.00	0.80
La	26.9	25.9	30.4	29.6	37.2	30.3	35.4	33.1	37.7	28
Lu	0.35	0.34	0.39	0.40	0.43	0.34	0.40	0.34	0.53	0.35
Nb	12.1	11.0	14.4	12.5	14.9	12.4	11.5	12.2	11.8	10.9
Nd	21.5	21.1	22.4	22.1	26.1	23.8	24.6	23.4	24.7	20.8
Pr	5.73	5.56	6.16	5.91	7.09	6.32	6.49	6.00	7.06	5.29
Rb	83.0	69.6	79.7	73.8	115.0	163.5	153.5	124.5	152.0	91.5
Sm	4.40	3.71	4.21	4.46	4.84	4.90	4.56	4.51	4.31	3.95
Sn	3	1>	3	2	3	4	5	4	5	3
Sr	367.0	338.0	369.0	359.0	284.0	268.0	276.0	332.0	73.3	289.0
Ta	1.0	0.9	1.1	1.0>	1.3	1.0>	1.0>	1.1	1.4	0.8
Tb	0.63	0.62	0.73	0.68	0.69	0.65	0.58	0.59	0.80	0.62
Th	11.60	10.25	12.65	11.45	18.00	15.35	21.50	17.95	27.70	12.35
Tm	0.34	0.37	0.44	0.38	0.41	0.36	0.36	0.40	0.52	0.42
U	2.39	2.04	2.58	2.35	4.26	2.99	4.27	3.52	5.15	2.96
V	93	77	83	87	56	68	48	67	6	31
W	1>	1>	1>	1>	4	2	3	2	3	5
Y	22.5	20.9	24.9	24.0	25.7	23.8	24.4	22.9	28.3	23.3
Yb	1.92	2.04	2.96	2.43	2.54	2.49	2.54	2.65	3.50	2.72
Zr	203	212	277	240	285	262	245	259	189	221

Table 1. Concentration of major oxides (in wt%) and trace elements (in ppm) in the analyzed rock samples.

Rock Type	Rhyolite						Basaltic trachy Andesite			Trachyte
Sample Name	T.S.P-55	T.F.V-34	T.F.V-38	T.F.CH-11	T.S.V-91	T.S.V-92	T.S.V-40	T.F.T-32	T.S.V-66	T.S.V-82
SiO_2	75.51	70.71	76.79	79.46	74.91	78.09	52.91	53.72	54.62	58.73
Al_2O_3	13.66	13.10	12.43	11.06	13.63	11.88	19.80	18.90	20.50	19.86
CaO	0.70	3.17	0.77	1.20	1.16	0.59	8.31	8.94	7.66	2.27
MgO	0.55	0.90	0.10		0.21	0.07	4.38	4.10	3.36	0.25
Na_2O	2.57	1.89	2.19	3.00	3.34	3.11	4.23	3.84	4.19	1.99
K_2O	5.13	8.50	7.01	4.08	4.96	5.05	1.70	1.55	1.84	9.70
Cr_2O_3	0.01	0.01	0.01	0.02	0.01	0.01	0.01	0.01	0.01	0.01
TiO_2	0.22	0.20	0.17	0.15	0.24	0.16	1.49	1.25	1.23	1.31
MnO	0.01	0.05	0.01	0.02	0.03	0.03	0.11	0.12	0.09	0.10
P_2O_5	0.03	0.04	0.05	0.04	0.03	0.01	0.41	0.38	0.33	0.41
SrO	0.01	0.01	0.01	0.01	0.01	0.01	0.06	0.06	0.05	0.01
BaO	0.03	0.03	0.03	0.03	0.03	0.04	0.04	0.04	0.05	0.11
Fe_2O_3	1.80	1.78	1.69	1.66	1.82	1.69	3.03	2.79	2.78	2.89
LOI	4.06	4.19	1.61	1.48	4.22	1.27	2.85	2.88	1.72	3.94
Ba	268	239	267	258	292	329	382	301	392	856
Ce	64.1	58.1	57.9	59.9	61.5	58.4	59.8	53.7	55.8	58.2
Cr	20	10	50	90	20	50	40	50	20	20
Cs	8.83	3.93	9.37	11.30	17.25	13.10	1.20	1.26	0.91	4.58
Dy	2.82	2.45	2.87	2.88	2.70	2.36	4.43	3.96	4.19	4.26
Er	1.87	1.69	1.81	2.06	1.78	2.10	2.62	2.30	2.38	2.33
Eu	0.49	0.37	0.40	0.38	0.45	0.42	1.60	1.42	1.40	1.34
Ga	13.4	13.3	12.8	11.4	13.7	12.0	20.1	19.4	19.5	19.0
Gd	2.71	2.53	2.63	2.88	2.52	2.33	4.57	4.35	4.65	4.82
Hf	4.2	3.9	3.8	3.9	4.1	3.5	4.7	4.7	4.7	4.4
Ho	0.57	0.55	0.57	0.63	0.54	0.52	0.94	0.74	0.81	0.84
La	37.1	32.8	33.2	35.7	35.1	33.7	29.7	26.9	29.3	28.4
Lu	0.32	0.31	0.34	0.43	0.37	0.38	0.35	0.30	0.32	0.30
Nb	12.0	10.4	10.6	10.0	11.6	10.5	16.5	13.4	14.9	13.8
Nd	19.1	16.8	17.9	18.7	19.1	16.6	24.9	23.4	21.6	23.9
Pr	5.70	5.24	5.62	5.79	5.58	5.15	6.16	5.74	5.74	6.04
Rb	171.5	203.0	202.0	144.5	278.0	174.0	30.6	31.9	46.2	222.0
Sm	2.74	2.63	2.86	3.00	3.17	2.49	4.33	4.48	4.22	4.58
Sn	4	3	4	4	4	4	1>	2	2	3
Sr	90.2	60.3	68.6	75.2	108.5	109.5	705.0	657.0	630.0	144.0
Ta	1.4	1.4	1.4	1.1	1.4	1.2	1.1	1.0>	1.0>	0.9
Tb	0.45	0.44	0.43	0.45	0.38	0.39	0.68	0.63	0.68	0.71
Th	34.80	31.30	30.00	28.00	31.00	30.10	6.43	6.49	7.12	9.77
Tm	0.35	0.30	0.29	0.36	0.33	0.32	0.35	0.36	0.34	0.36
U	5.19	3.92	4.84	6.08	6.21	6.27	1.24	0.92	1.45	1.99
V	12	9	10	7	15	8	201	192	127	109
W	3	3	2	6	3	4	1>	1>	1>	2
Y	16.8	16.3	18.0	19.6	17.6	17.6	23.0	20.7	22.2	23.4
Yb	2.13	1.81	2.05	2.33	2.01	2.50	2.31	2.06	2.39	2.20
Zr	147	138	154	120	151	140	227	186	231	211

According to the Harker diagrams (Fig 5), by increasing the content of SiO_2, the values of all major oxides except for K_2O decreased. The value of K_2O rises with increasing the SiO_2 content. However, variation in Na_2O concentration can be a result of alteration in the parent rocks. The content of MgO in the andesites ranges from 2.52 to 2.96 wt%, with the Mg# of 51.04 to 55.74 indicating a high value for these rocks according to Qian et al. (2017) (Fig 4d). Mg# was calculated based on the following formula:

$$Mg\# = [MgO/(MgO+FeO^t)] \times 100.$$

Fig 6 illustrates the variation of trace elements against SiO_2 content. As it is evident here, Y, Nb, Zr, Sr contents decrease with increasing SiO_2 reflecting the trend of fractional crystallization.

According to the chondrite-normalized REE spider diagram (Boynton 1984), various rocks of the study area display a relatively smooth parallel trend for REE patterns (Fig 7a) indicating the same petrogenetic processes. Apparently, most rhyolite and some dacite samples represent a negative anomaly for Eu. With regard to the primitive mantle-normalized spider diagram (Sun and McDonough 1989), the rocks are enriched in LILEs and are depleted in HFSEs (e.g. Nb-Ti) showing negative anomalies of Sr and P (Fig 7b). The remarkable negative anomaly of Nb, Ti, Eu, Sr in acidic and intermediate lavas including andesite, dacite and rhyolite is comparable with that in calc-alkaline subduction-related lavas (Kuscu and Geneli 2010; Litvak et al. 2015; Yang et al. 2015; Qian et al. 2016 and 2017; Ersoy et al. 2017).

When plotted on 100 Th/Zr versus 100Nb/Zr diagram (Pearce 1983), all of the rock samples fall in subduction-related volcanic arc field (Fig 8a). The samples are plotted within the subduction setting and the active continental margin fields on the basis of Ta/Yb versus Th/Yb diagram (Pearce 1983) (Fig 8b).

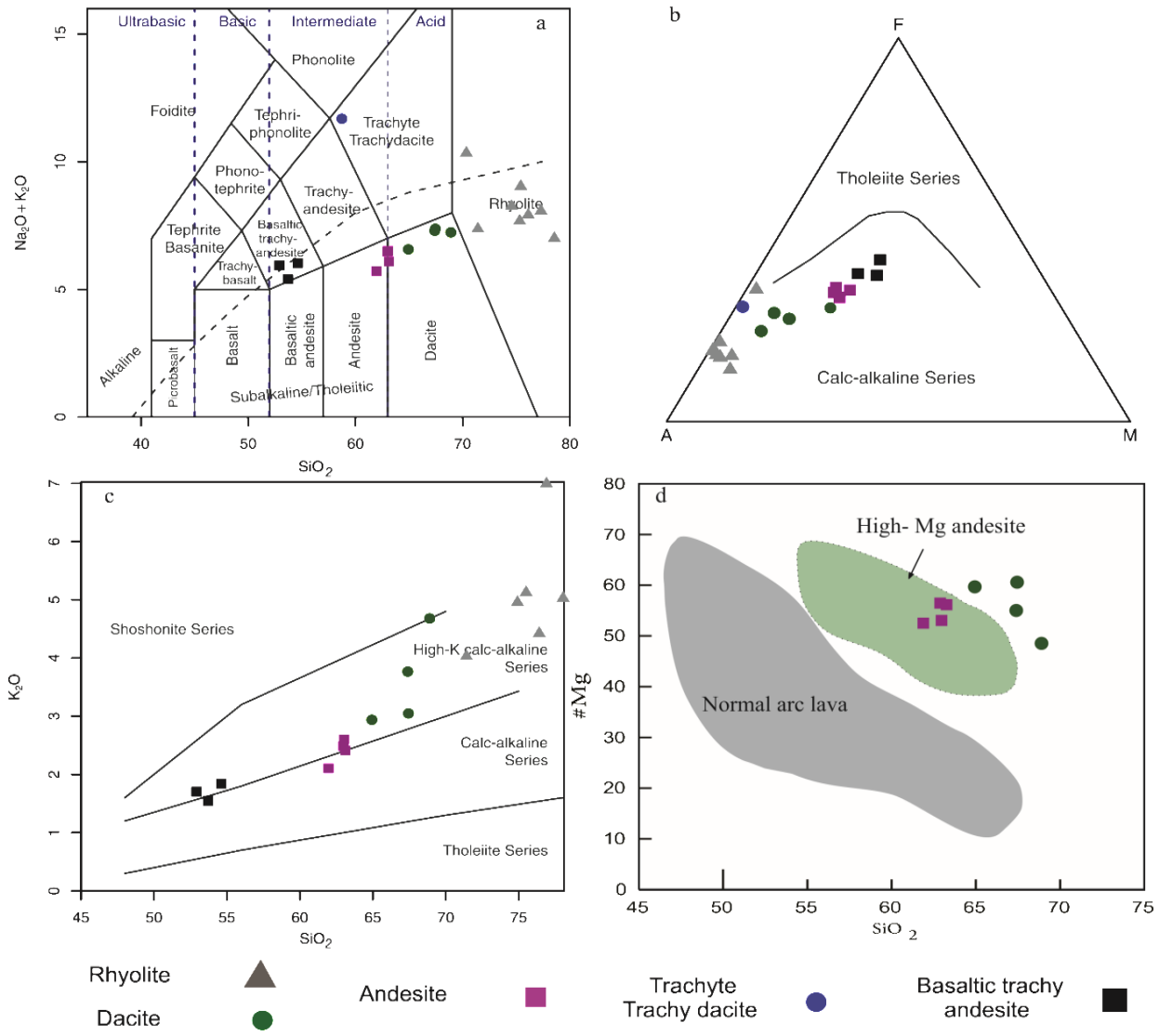

Fig 4. Geochemical classification diagrams: a) Na_2O+K_2O vs SiO_2 (Le Bas et al. 1986), b) FeO-MgO- ($Na_2O + K_2O$) (Irvine and Baragar 1971), c) SiO_2 vs K_2O (Peccerillo and Taylor 1976), d): SiO_2 vs Mg# (after Kelemen 1995 and Qian et al. 2017).

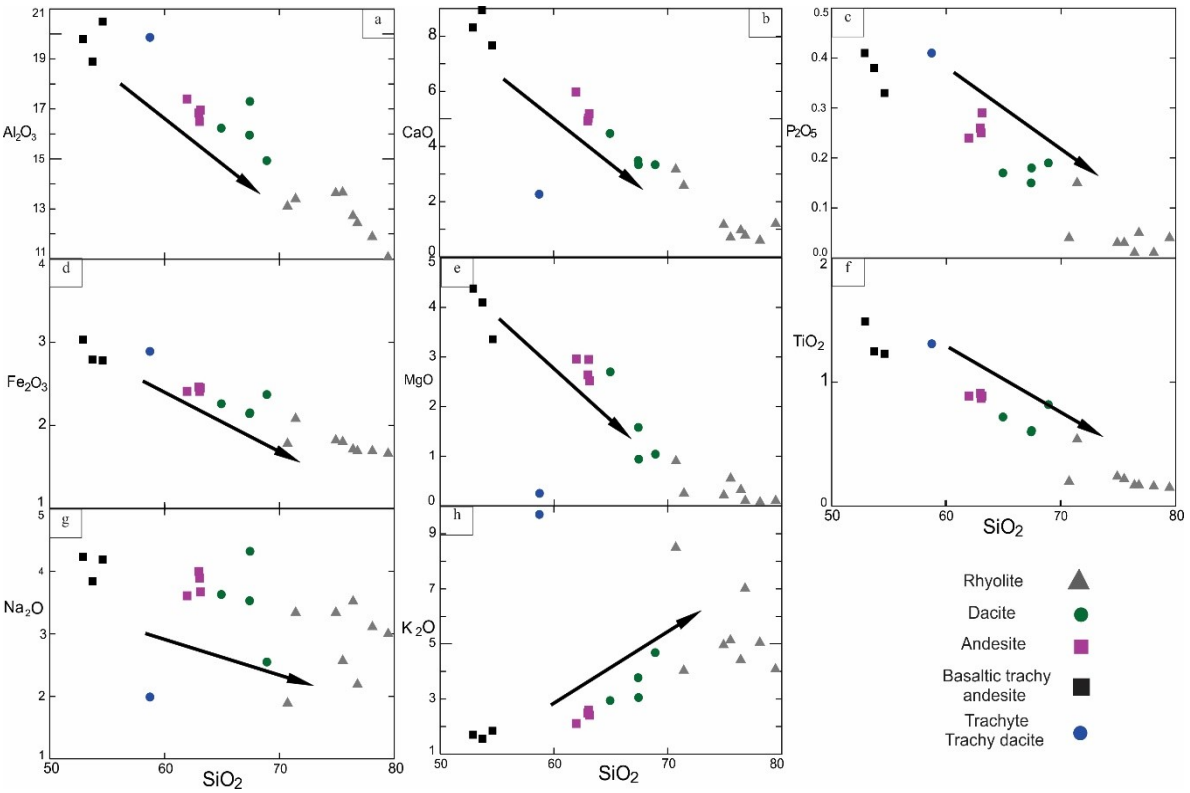

Fig 5. Plots of silica contents vs Major oxides of rock samples a) Al_2O_3, b) CaO, c) P_2O_5, d) Fe_2O_3, e) MgO, f) TiO_2, g) Na_2O_3, h) K_2O.

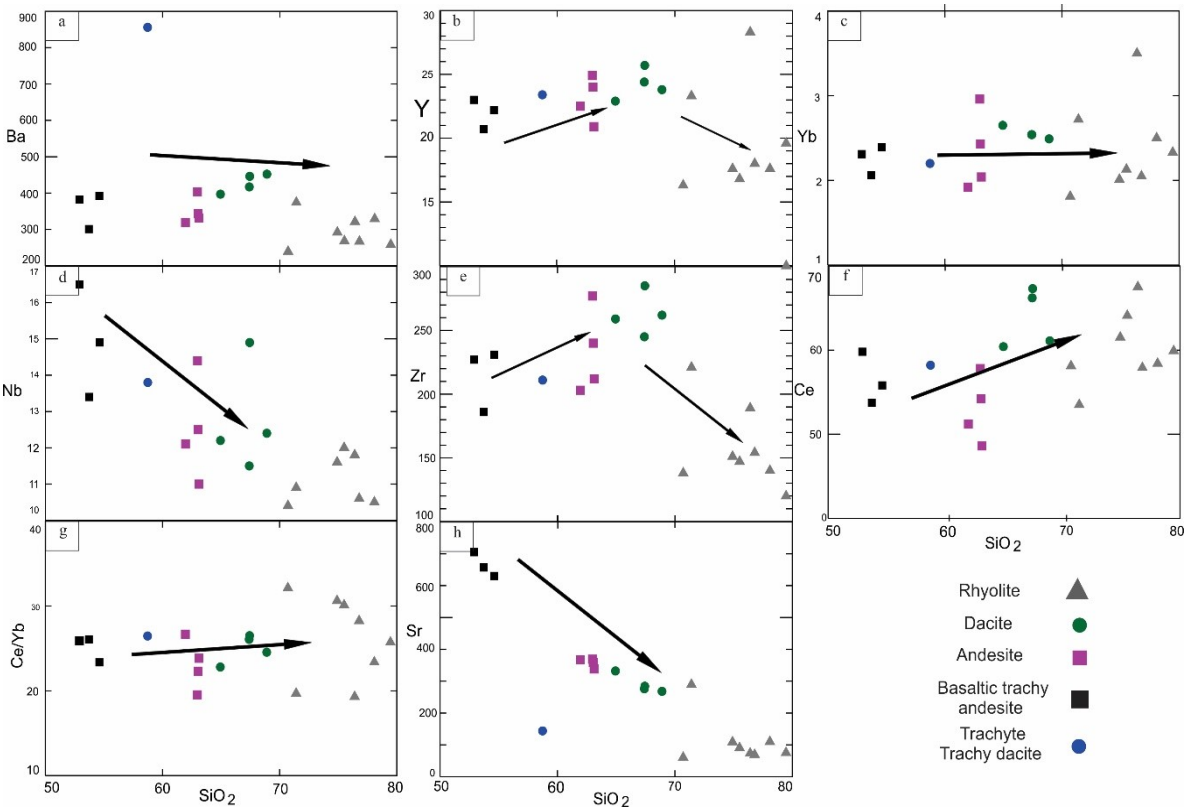

Fig 6. Plots of silica contents of rock samples vs a) Ba, b) Y, c) Yb, d) Nb, e) Zr, f) Ce, g) Ce/Yb and h) Sr.

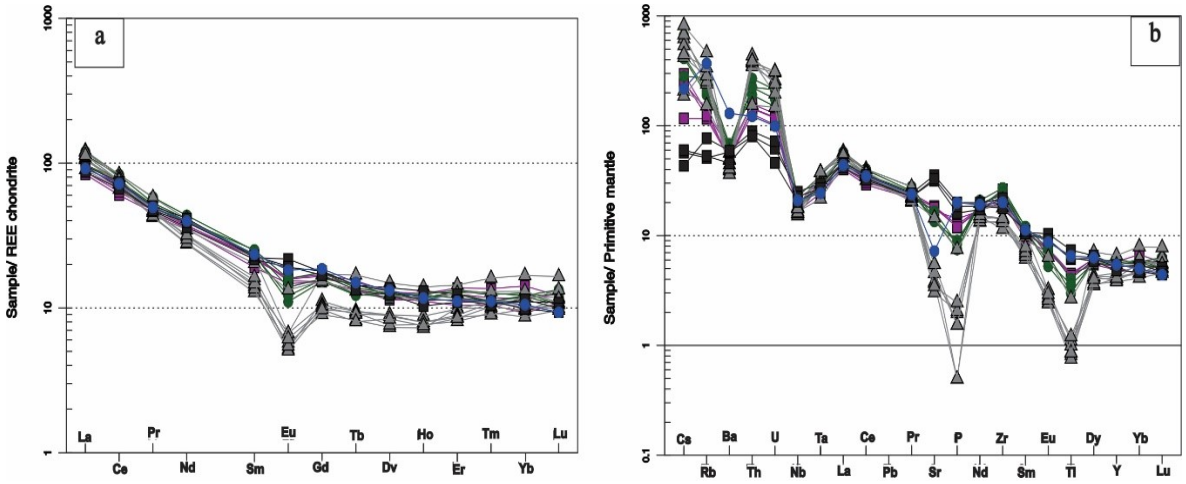

Fig 7. a) Primitive mantle-normalized trace element spider diagram (Sun and McDonough 1989) and b) Chondrite-normalized REE patterns (Boynton 1984).

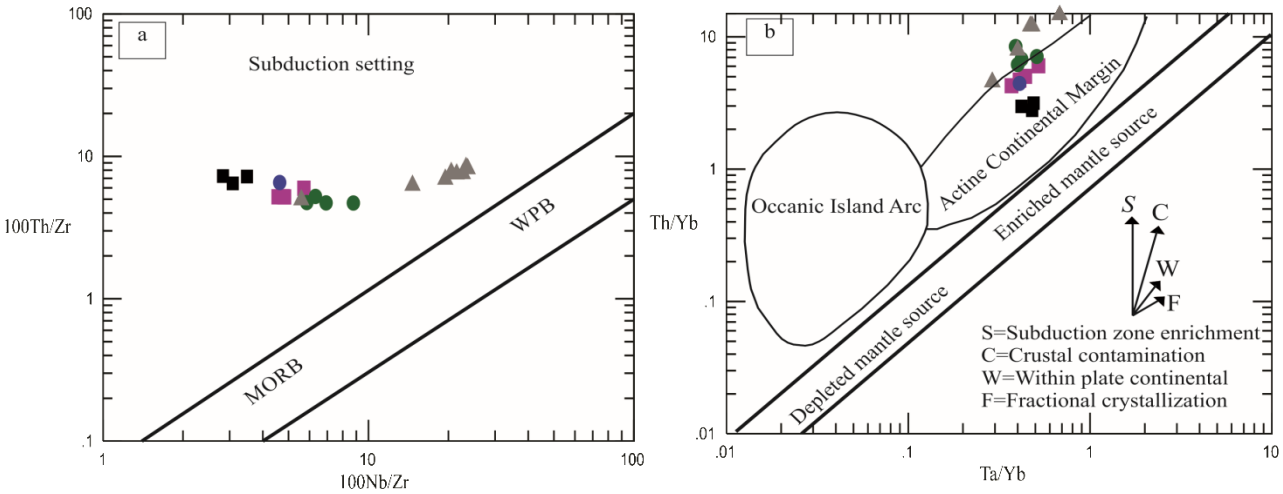

Fig 8. 100Th/Zr vs. 100Nb/Zr diagram and Ta/Yb vs. Th/Yb diagram, after Pearce (1983).

6. Discussion

6.1. Fractional crystallization and crustal contamination

The mineralogy of a volcanic suite reflects the processes occurring during their petrogenesis and subsequent events such as fractional crystallization, magma mixing and contamination, Fractional crystallization and partial melting processes with or without crustal contamination (FC-AFC) have crucial roles in the petrogenesis of intermediate calc-alkaline rocks in subduction zones (Çoban et al. 2012; Pang et al. 2013; Liu et al. 2014; Long et al. 2015; Yang et al. 2015; Litvak et al. 2015; Qian et al. 2016 and 2017; Chazot et al. 2017; Ersoy et al. 2017).

According to the geochemical data in this study, fractional crystallization trend was proved by the binary diagrams of major element oxides versus SiO_2 (Fig 4), major and trace elements and petrographic studies (Fig 3) which is shown by a decrease in the content of MgO, FeO_t, CaO, TiO_2, Al_2O_3, NaO_2, with increasing SiO_2. These evidence reflect the fractional crystallization process associated with the crystallization of plagioclase, pyroxene, feldspar, iron oxide, and titanium.

The fractional crystallization of plagioclase is also indicated by a decreasing trend in SiO_2 versus Sr/Y diagram (Fig 9) which has been also indicated by Aydınçakır (2014) in NE Turkey.

The proportion of trace and rare earth element contents reflects the separation of the minerals segregated from the parent magma after melting and through the fractionation or assimilation and contamination processes (Litvak et al. 2015). Decrease in the content of TiO_2 and P_2O_5 along with the increasing the concentration of SiO_2 (Fig 4) and the negative anomaly of Ti (Fig 7) are attributed to the partial fractionation of iron oxide, titanium oxide and apatite. (Qian et al. 2016)

referred to the same point for rock series in Chiang Khong, NW Thailand.

Depletion of Ba (Fig 7) implies the fractionation of feldspars (Arslan and Aslan 2006) and negative anomalies of Eu and Sr (Fig 7) indicate the partial fractionation of the plagioclases (Qian et al. 2016 and 2017). These evidence suggested that the intermediate to acidic volcanic rocks in the study area were formed through the fractional crystallization.

The presence of crustal components in the subduction zone rock series with an intermediate calc-alkaline affinity has been attributed to several factors including: 1) partial melting of the continental crust (Long et al. 2015), 2) partial melting and recycling of sediments on descending subducting slab (Qian et al. 2016 and 2017), 3) delamination of crust and asthenosphere upwelling (Yang et al. 2014 and 2015; Ersoy et al. 2017), 4) descending slab break–off and its impact on the inherited mantle source (Pang et al. 2012 and 2013).

The ratio of Zr/Nb>10 represents a magmatism related to a mantle source modified by subduction processes (Sommer et al. 2006). This ratio changes from 12 to 20 in the rocks of the study area so that, strongly reflects the influencing subduction processes. The ratios of Nb/La and Nb/U are the indicators sensitive to crustal contamination (Hofmann et al. 1986; Furman 2007) which are normally 0.39 and 4.4 in the crust and 0.9-1/3 and 50 in the mantle respectively (Hofmann et al. 1986; Sun and McDonough 1989; Rudnick and Gao 2004). The analyzed rocks of Momen Abad have revealed the values of Nb/La=0.56 to 0.28 and Nb/U=1.67 to 14.57 which admit the influence of crustal contamination clearly. Nb/Y is found to be below 1.72 in the active continental margins (Temel et al. 1998) and the studied samples showed the variation below 1 for this parameter.

According to the Nb/Y versus Rb/Y diagram (Temel et al. 1998), the samples are enriched in the subduction zone and experienced crustal contamination (Fig 10b).

Rb versus Ba/Rb diagram (Fig 10b) (Askren et al. 1997) clarifies the role of crustal contamination associated with the fractional crystallization in the upper crust.

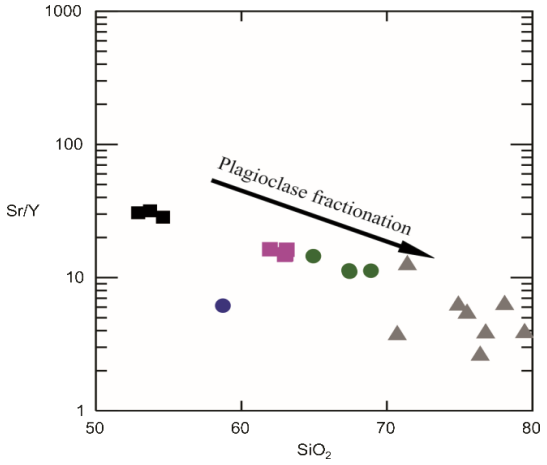

Fig 9. Momen Abad rock samples plotted on the SiO_2 vs Sr/Y diagram (Aydınçakır 2014) showing an obvious fractionation of plagioclase minerals.

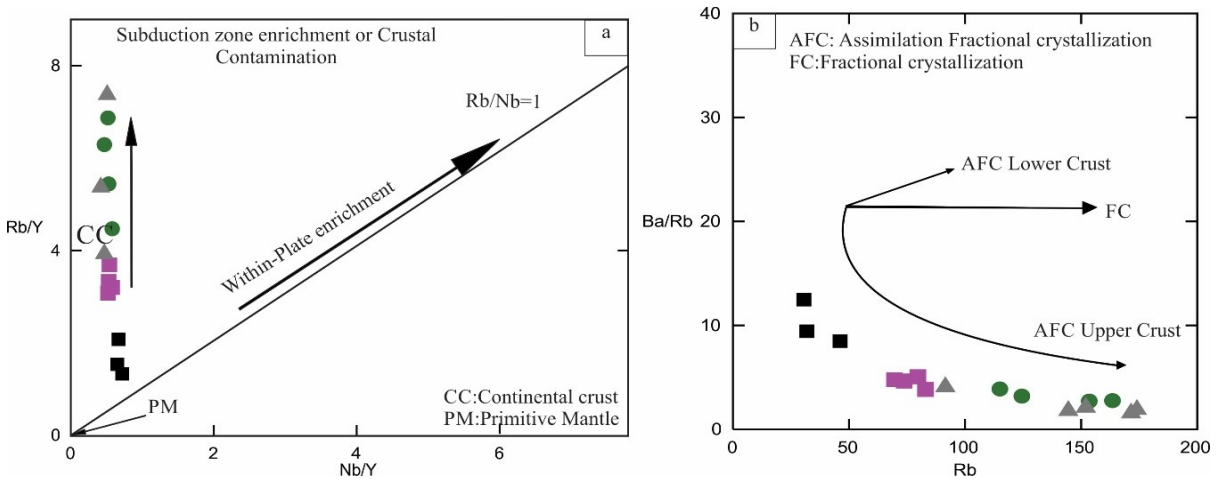

Fig 10. Momen Abad rock samples plotted on a) Nb/Y vs. Rb/Y diagram (Temel et al. 1998); b) Rb vs. Ba/Rb diagram (Askren et al. 1997).

6.2. Mantle source and enrichment processes

The low Nb/La and Nb/Ba ratios (<0.47 and 0.02, respectively) are attributed to the asthenospheric mantle sources enriched by the subduction-related metasomatic processes (Ersoy et al. 2017). This is not the case in Momen Abad region as the ratios of Nb/La and Nb/Ba are below 0.6 and 0.05 respectively. The Nb/Ba and Nb/Zr ratios (Fig 11a) (Hooper and Hawkesworth 1993) disclose that Momen Abad volcanic rocks are related to the sub-continental lithosphere.

The processes occurring in the subduction zone in the study area are illustrated by the anomalies of Nb, Ti, Eu and Sr depicted in the chondrite-normalized and primitive mantle-normalized spider diagrams. Moreover, the Th/Yb versus Nb/Yb diagram (Pearce 2008 and After Ersoy et al. 2017) displays the mantle array enriched by the involvement of the subduction zone components (Fig 11b). Mineralogical composition of the mantle source is an important factor in the partial melting (whether it contains spinel or garnet) (Ersoy et al. 2017). In subduction-related areas, melts with the residual garnets in magma source are remarkably depleted in HREEs, so that Y and Yb are below 15 and 1.4 ppm, respectively (Drummond and Defant 1990). These values are between 16.3 and 25.7 (for Y) and 3.5 and 1.81 ppm (for Yb) in Momen Abad rocks which approve the absence of residual garnets. Besides, Th/Yb versus La/Yb diagram (Ersoy et al. 2017) confirms the mantle enrichment trend and the presence of spinel lherzolite phase as well as the absence of residual garnets in the magma source of Momen Abad rocks (Fig 11c).

The ratio of HFSE and REE elements, for instance Nb/Yb and Zr/Yb versus Ta/Yb are commonly used to deduce the parent magma sources (Pang et al. 2013) which shows an E-MORB-like mantle source for the Momen Abad area (Fig 12a, b).

Moreover, the values of Zr/Nb in N-MORB and E-MORB are 32 and 9, respectively (Sun and McDonough 1989). However, this ratio is about 12 in Momen Abad area showing that the rocks of the study area were derived from an E-MORB mantle source.

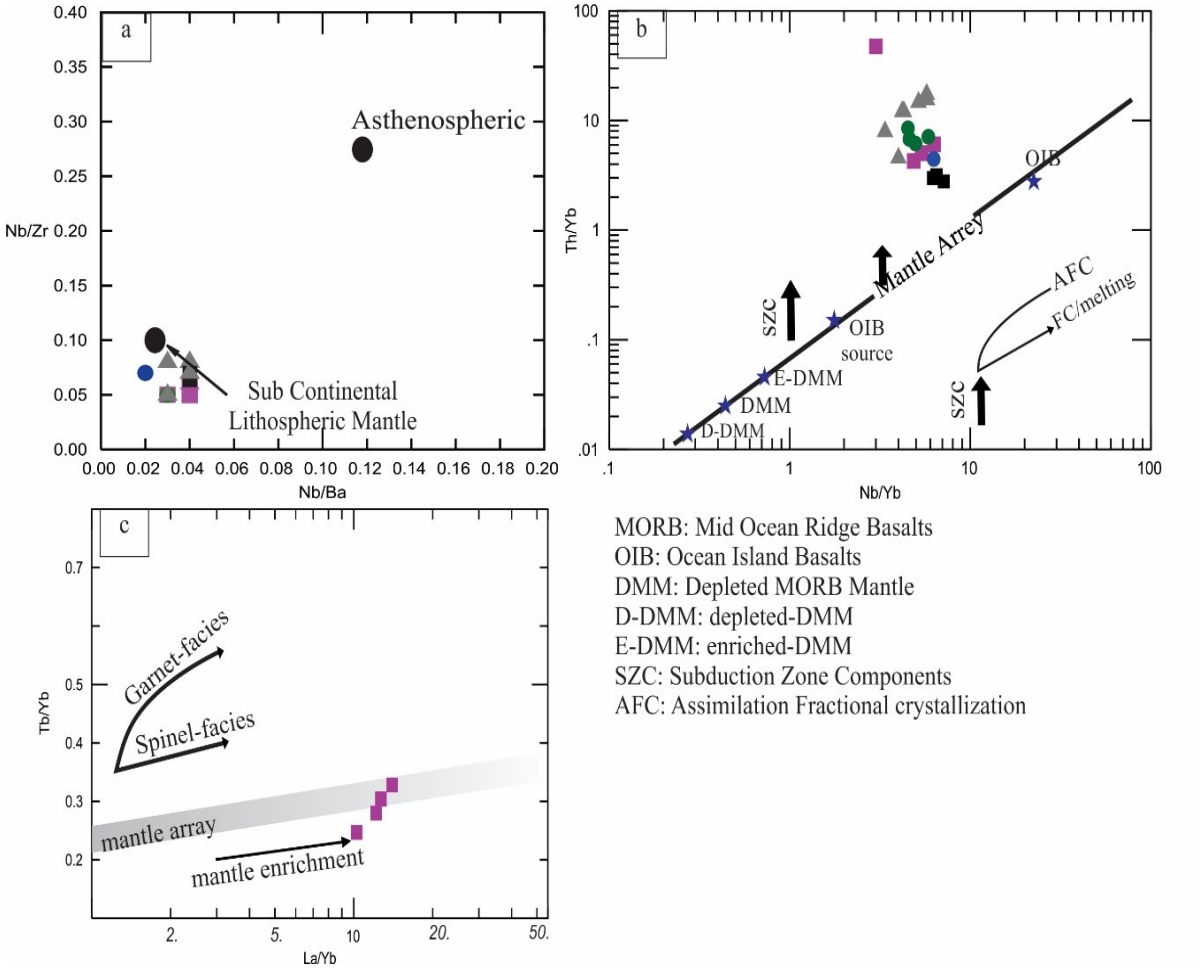

Fig 11. Momen Abad samples plotted on a) Nb/Ba vs Nb/Zr diagram (Hooper and Hawkesworth 1993); b) Th / Yb vs Nb/Yb diagram (Pearce 2008 and after Ersoy et al. 2017); c) Th/Yb vs La/Yb diagram (Ersoy et al. 2017).

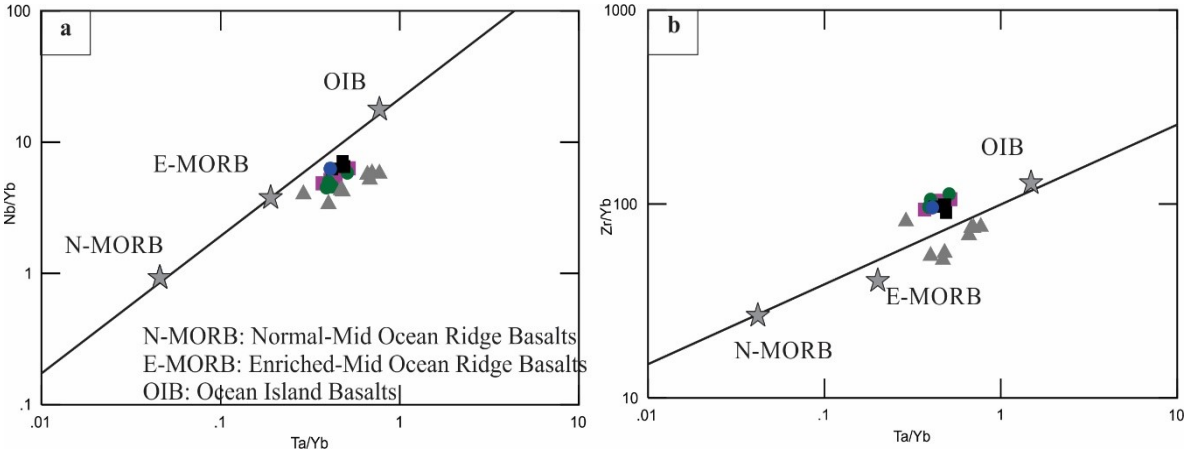

Fig 12. Momen Abad samples plotted on a) Nb/Yb vs Ta/Yb an\d b) Zr/Yb vs Ta/Yb diagrams (Pang et al. 2013).

6.3. Modified mantle source

Partial melting of the subducted crustal materials is the most important controlling factor in producing metasomatized mantle (Labanieh et al. 2012; Yang et al. 2014 and 2015). The subducted slab and its accompanied sediments release hydrous fluids resulting in a partial melting in the mantle wedge and subsequently the migration of LILE and LREE (Pearce and Peate 1995; Hoang et al. 2011). The high ratio of Th/Yb can be ascribed to a source which is metasomatized during the subduction-related enrichment and/or associated with crustal contamination (Kuscu and Geneli 2010). The amount of Th in the subducted regions is controlled by the cycling of sediments (Yang et al. 2015) and the high ratio of Th/Nb in the subduction-related lavas confirms the cycling and melting of sediments (Qian et al. 2016 and 2017; Ersoy et al. 2017).

The Ba/Nb versus Th/Nb diagram (Ersoy et al. 2010) illustrates the metasomatism of melted sediments**,** metasomatic fluids and the role of rutile in the mantle source region (Fig 13a). The Ba/La versus Th/Yb diagram (after Wang et al. 2010 and Qian et al. 2017) explains the cycling of subduction-related sediments and indicates the metasomatizing fluids derived from the subducted zone (Fig 13b). The Ba/Th versus Th/Nb diagram (Orozco-Esquivel et al. 2007) elucidates melting of the lower crust and upper crusts' sediments (Fig 13c).

Considering the changes in the content of elements and their ratio in the studied samples, it is supposed that metasomatism is related to the melting of the upper crust's sediments and not to the fluids released. This is due to the subduction under the Lut Block and variation in the composition of the subducting slab. Therefore, the composition of the mantle sources in the subduction area of Momen Abad changes as a function of fractional crystallization, partial melting, mantle metasomatism, melting of sediments and contamination by the subducting materials.

6.4. The petrogenesis of andesite - dacite and rhyolite in the study area

Several petrogenetic models were accounted for the generation of intermediate to acidic magmas by scholars around the world and the most relevant models are pointed out here. It has been proposed that high-Mg# andesites are formed mainly through: 1) partial melting of an eclogitic and granolitic crust, 2) partial melting of a young and hot subducting slab with adakitic nature (Qian et al. 2016 and 2017; and the references cited in).

The partial melting of an eclogitic-granolitic crust requires a low-rutile and low Mg# with Al_2O_3>17% (Qian et al. 2017). However, high Mg content (0.94-2.96%) and high Mg# (51.04 to 55.74), Al_2O_3<17% refuses the partial melting of an eclogitic crust in this area. The partial melting of a young subducting slab with adakitic nature is defined by Sr, Al and Si values >400 ppm, Y<18 ppm, and Yb <1.9 ppm (Qian et al. 2017). But Sr is <400, Y>20 and Yb is >1.9 up to 2.96 ppm. So this cannot be considered as the source of andesite-dacite in the study area.

The isotopic studies of Sistan-Lut volcanic rocks, especially in Birjand, Sarbisheh, and Sarchah regions by Elahpour et al. (2016) and Pang et al. (2013) showed $^{87}Sr/^{86}Sr$ ratios of 0.704-0.706‰ for andesites and dacites and 0.704-0.711‰ for rhyolites. The $^{143}Nd/^{144}Nd$ isotopic ratios is about 0.512‰. These authors suggested lithospheric mantle melting was the origin of the volcanic rocks in Birjand and Sarbisheh and indicate an enrichment resulted from lithospheric plate subduction and crustal material metasomatism. Elahpour et al. (2016) focused on the crustal contamination in petrogenesis of rhyolites and other acidic rocks based on the aforementioned isotopic ratios.

Metasomatism related to the fluids liberated from the subducting oceanic slab is characterized by negative Nb anomaly and high ratios of Ba/Th and Ba/La. On the other hand, the metasomatism related to the sediments over the subduction plate is associated with high Th and high ratios of Th/Yb and Th/Nb (Yang et al. 2015; Qian

et al. 2017). Regarding the lack of Nb anomaly, high Th content (10-22), low Ba/Th (19-32), Th/Yb = 4.71-8.46 and Th/Nb = 0.88-1.87, a mantle source modified by the recycled sediments and subducting slab is suggested for andesite and dacites.

According to the aforementioned evidence provided here, the high Mg# andesite volcanic rocks had not originated from partial melting of eclogitic and granolitic crust and the subducting young oceanic slab with adakitic affinity. So that, these rocks and also high silica rhyolitic rocks were formed from MORB like mantle components and partial melting of subcontinental lithospheric mantle. The subducting crust components and recycling of upper crust sediments had also significant roles in producing a modified mantle source. Therefore, the petrogenesis of this area discloses partial melting of a source, metasomatized by recycled sediments of subducting slab and a source close to the modified mantle which has been evidenced by Qian et al. (2016 and 2017).

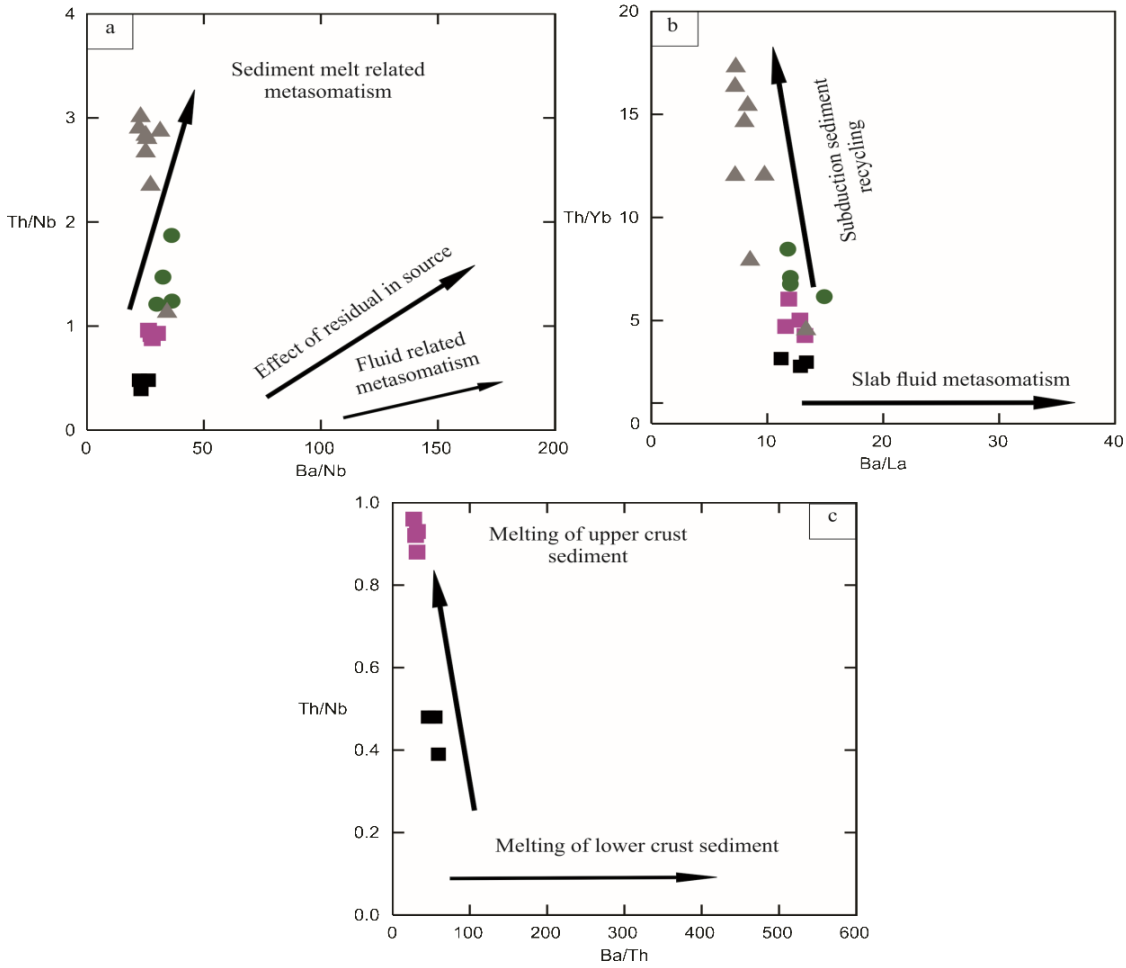

Fig 13. Momen Abad samples plotted on a) Ba/Nb vs Th/Nb diagram (Ersoy et al. 2010), b) Ba/La vs Th/Yb diagram (after Wang et al. 2010 and Qian et al. 2017), c) Ba/Th vs Th/Nb diagram (Orozco-Esquivel et al. 2007).

7. Conclusion

Petrographic and geochemical studies showed that the volcanic rocks of the study area are intermediate to acidic in composition. They are intermediate to high-K calc-alkaline rocks of Cenozoic age including andesite-trachyandesite, dacite and rhyolite. Calc-alkaline lavas of this area indicate a subduction zone and active continental margin setting which are relatively enriched in LILE and LREE elements compared to HREE and HFSE elements and they are depleted in Nb, Ti, Sr, P and Eu. The geochemical characteristics of the intermediate to acidic rocks of Momen Abad area indicate that they have originated by fractional crystallization of a subcontinental lithospheric mantle, an E-MORB like source with spinel lherzolite composition. The fractional crystallization is inferred by evidences like phenocrysts

of plagioclase, alkali feldspar, quartz, pyroxene, amphibole, and biotite and also the trends of major oxides and trace elements plotted in relevant diagrams against SiO_2. According to the presence of LILE, REE and HFSE and trace element ratios the fractional crystallization and contamination of upper crust (AFC) has affected the source of andesites, dacites and rhyolites in Momen Abad. High ratios of HFSE and REE Th and elevated contents of Th represent a modified metasomatized mantle deriving from the subducting and melting of the upper crust during the subduction of Neotethys ocean beneath the Lut Block.

References

Arjmandzadeh R, Karimpour MH, Mazaheri S A, Santos J, Medina J, Homam SM (2011) Sr–Nd isotope geochemistry and petrogenesis of the Chah-Shaljami granitoids (Lut block, eastern Iran). *Journal of Asian Earth Sciences 41*(3): 283-296.

Arslan M, Aslan Z (2006) Mineralogy, petrography and whole-rock geochemistry of the Tertiary granitic intrusions in the Eastern Pontides, Turkey. *Journal of Asian Earth Sciences 27*(2): 177-193.

Askren DR, Roden MF, Whitney JA (1997) Petrogenesis of Tertiary andesite lava flows interlayered with large-volume felsic ash-flow tuffs of the western USA. *Journal of Petrology 38*(8): 1021-1046.

Aydınçakır E (2014) The petrogenesis of Early Eocene non-adakitic volcanism in NE Turkey: Constraints on the geodynamic implications. *Lithos 208-209*: 361-377.

Berberian M (1983) Continental deformation in the Iranian Plateau. *Rep./Iran. Geol. survey*.

Boynton WV (1984) Cosmochemistry of the rare earth elements: meteorite studies *Developments in geochemistry*. Elsevier 2: 63-114.

Camp V, Griffis R (1982) Character, genesis and tectonic setting of igneous rocks in the Sistan suture zone, eastern Iran. *Lithos 15*(3): 221-239.

Chazot G, Abbassene F, Maury RC, Déverchère J, Bellon H, Ouabadi A, Bosch D (2017) An overview on the origin of post-collisional Miocene magmatism in the Kabylies (northern Algeria): Evidence for crustal stacking, delamination and slab detachment. *Journal of African Earth Sciences 125*: 27-41.

Çoban H, Karacık Z, Ece ÖI (2012) Source contamination and tectonomagmatic signals of overlapping Early to Middle Miocene orogenic magmas associated with shallow continental subduction and asthenospheric mantle flows in Western Anatolia: A record from Simav (Kütahya) region. *Lithos 140*: 119-141.

Drummond MS, Defant MJ (1990) A model for trondhjemite, tonalite, dacite genesis and crustal growth via slab melting: Archean to modern comparisons. *Journal of Geophysical Research: Solid Earth 95*(B13): 21503-21521.

Ersoy EY, Helvacı C, Palmer MR (2010) Mantle source characteristics and melting models for the early-middle Miocene mafic volcanism in Western Anatolia: implications for enrichment processes of mantle lithosphere and origin of K-rich volcanism in post-collisional settings. *Journal of Volcanology and Geothermal Research 198*(1): 112-128.

Elahpour E, Vosoughi Abedini M, Pourmoafi SM (2016) Determination of parental melt nature and evolutions of volcanic rocks in Sarchah geological map area (southern Khorasan) based on isotopic data. *Iranian Journal of Geology* 10 (38): 103-113.

Ersoy EY, Palmer MR, Genç ŞC, Prelević D, Akal C, Uysal İ (2017) Chemo-probe into the mantle origin of the NW Anatolia Eocene to Miocene volcanic rocks: Implications for the role of, crustal accretion, subduction, slab roll-back and slab break-off processes in genesis of post-collisional magmatism. *Lithos 288*: 55-71.

Furman T (2007) Geochemistry of East African Rift basalts: an overview. *Journal of African Earth Sciences 48*(2-3): 147-160.

Hoang N, Itoh Ji, Miyagi I (2011) Subduction components in Pleistocene to recent Kurile arc magmas in NE Hokkaido, Japan. *Journal of Volcanology and Geothermal Research 200*(3): 255-266.

Hofmann A, Jochum K, Seufert M, White W (1986) Nb and Pb in oceanic basalts: new constraints on mantle evolution. *Earth and Planetary science letters 79*(1-2): 33-45.

Hooper P, Hawkesworth C (1993) Isotopic and geochemical constraints on the origin and evolution of the Columbia River basalt. *Journal of Petrology 34*(6): 1203-1246.

Irvine T, Baragar W (1971) A guide to the chemical classification of the common volcanic rocks. *Canadian journal of earth sciences 8*(5): 523-548.

Kuscu GG, Geneli F (2010) Review of post-collisional volcanism in the Central Anatolian Volcanic Province (Turkey), with special reference to the Tepekoy Volcanic Complex. *International Journal of Earth Sciences 99*(3): 593-621.

Kelemen PB (1995) Genesis of high Mg andesites and the continental crust. *Contributions to Mineralogy and Petrology* 120: 1–19.

Labanieh S, Chauvel C, Germa A, Quidelleur X (2012) Martinique: a clear case for sediment melting and slab dehydration as a function of distance to the trench. *Journal of Petrology 53*(12): 2441-2464.

Le Bas ML, Maitre RL, Streckeisen A, Zanettin B, IUGS Subcommission on the Systematics of Igneous Rocks (1986) A chemical classification of volcanic rocks based on the total alkali-silica diagram. Journal of petrology 27(3): 745-750.

Litvak VD, Spagnuolo MG, Folguera A, Poma S, Jones RE, Ramos VA (2015) Late Cenozoic calc-alkaline volcanism over the Payenia shallow subduction zone,

South-Central Andean back-arc (34° 30′–37° S), Argentina. *Journal of South American Earth Sciences 64*: 365-380.

Liu HQ, Xu YG, Tian W, Zhong YT, Mundil R, Li XH, . . . Shang-Guan SM (2014) Origin of two types of rhyolites in the Tarim Large Igneous Province: Consequences of incubation and melting of a mantle plume. *Lithos 204*: 59-72.

Long X, Wilde SA, Wang Q, Yuan C, Wang XC, Li J, . . . Dan W (2015) Partial melting of thickened continental crust in central Tibet: Evidence from geochemistry and geochronology of Eocene adakitic rhyolites in the northern Qiangtang Terrane. *Earth and Planetary Science Letters 414*: 30-44.

Nazari H, Salamati R (1999) Geological map of Sarbisheh (1/100000): Sheet.

Orozco-Esquivel T, Petrone CM, Ferrari L, Tagami T, Manetti P (2007) Geochemical and isotopic variability in lavas from the eastern Trans-Mexican Volcanic Belt: slab detachment in a subduction zone with varying dip. *Lithos 93*(1): 149-174.

Pang KN, Chung SL, Zarrinkoub MH, Khatib MM, Mohammadi SS, Chiu HY, . . .Lo CH (2013) Eocene–Oligocene post-collisional magmatism in the Lut–Sistan region, eastern Iran: magma genesis and tectonic implications. *Lithos 180*: 234-251.

Pang KN, Chung SL, Zarrinkoub MH, Mohammadi SS, Yang HM, Chu CH, . . . Lo CH (2012) Age, geochemical characteristics and petrogenesis of Late Cenozoic intraplate alkali basalts in the Lut–Sistan region, eastern Iran. *Chemical Geology 306*: 40-53.

Pearce JA (1983) Role of the sub-continental lithosphere in magma genesis at active continental margins.

Pearce JA (2008) Geochemical fingerprinting of oceanic basalts with applications to ophiolite classification and the search for Archean oceanic crust. *Lithos 100*(1-4): 14-48.

Pearce JA, Peate DW (1995) Tectonic implications of the composition of volcanic arc magmas. *Annual Review of Earth and Planetary Sciences 23*(1): 251-285.

Peccerillo A, Taylor SR (1976) Geochemistry of Eocene calc-alkaline volcanic rocks from the Kastamonu area, northern Turkey. *Contributions to mineralogy and petrology 58*(1): 63-81.

Qian X, Wang Y, Feng Q, Zi JW, Zhang Y, Chonglakmani C (2016) Petrogenesis and tectonic implication of the Late Triassic post-collisional volcanic rocks in Chiang Khong, NW Thailand. *Lithos 248*: 418-431.

Qian X, Wang Y, Srithai B, Feng Q, Zhang Y, Zi JW, He H (2017) Geochronological and geochemical constraints on the intermediate-acid volcanic rocks along the Chiang Khong–Lampang–Tak igneous zone in NW Thailand and their tectonic implications. *Gondwana Research 45*: 87-99.

Rudnic RL, Gao S (2004) Composition of the continental crust. In: Holland, H.D. and Turekian, K.K., Eds., Treatise on Geochemistry, Vol. 3, *The Crust, Elsevier-Pergamon, Oxford* 1-64.

Saccani E, Delavari M, Beccaluva L, Amini S (2010) Petrological and geochemical constraints on the origin of the Nehbandan ophiolitic complex (eastern Iran): Implication for the evolution of the Sistan Ocean. *Lithos 117*(1-4): 209-228.

Sommer CA, Lima EF, Nardi LV, Liz JD, Waichel BL (2006) The evolution of Neoproterozoic magmatism in Southernmost Brazil: shoshonitic, high-K tholeiitic and silica-saturated, sodic alkaline volcanism in post-collisional basins. *Anais da Academia Brasileira de Ciências 78*(3): 573-589.

Stocklin J (1968) Structural history and tectonics of Iran: a review. *AAPG Bulletin 52*(7): 1229-1258.

Sun SS, McDonough WS (1989) Chemical and isotopic systematics of oceanic basalts: implications for mantle composition and processes. *Geological Society, London, Special Publications 42*(1): 313-345.

Temel A, Gündoğdu MN, Gourgaud A (1998) Petrological and geochemical characteristics of Cenozoic high-K calc-alkaline volcanism in Konya, Central Anatolia, Turkey. *Journal of Volcanology and Geothermal Research 85*(1): 327-354.

Tirrul R, Bell I, Griffis R, Camp V (1983) The Sistan suture zone of eastern Iran. *Geological Society of America Bulletin 94*(1): 134-150.

Verdel C, Wernicke BP, Hassanzadeh J, Guest B (2011) A Paleogene extensional arc flare-up in Iran. *Tectonics 30*(3).

Wang YJ, Zhang AM, Fan WM, Peng TP, Zhang FF, Zhang YH, Bi XW (2010) Petrogenesis of late Triassic post-collisional basaltic rocks of the Lancangjiang tectonic zone, southwest China, and tectonic implications for the evolution of the eastern Paleotethys: *geochronological and geochemical constraints. Lithos* 120: 529–546.

Yang WB, Niu HC, Shan Q, Chen HY, Hollings P, Li NB, . . .Zartman RE (2014) Geochemistry of primary-carbonate bearing K-rich igneous rocks in the Awulale Mountains, western Tianshan: Implications for carbon-recycling in subduction zone. *Geochimica et Cosmochimica Acta 143*: 143-164.

Yang WB, Niu HC, Cheng LR, Shan Q, Li NB (2015) Geochronology, geochemistry and geodynamic implications of the Late Mesozoic volcanic rocks in the southern Great Xing'an Mountains, NE China. *Journal of Asian Earth Sciences 113*: 454-470.

Zarrinkoub MH, Pang KN, Chung SL, Khatib MM, Mohammadi SS, Chiu HY, Lee HY (2012) Zircon U–Pb age and geochemical constraints on the origin of the Birjand ophiolite, Sistan suture zone, eastern Iran. *Lithos 154*: 392-405.